

OVERVIEW OF CERAMICS PROJECT

R. Bruce Thompson  
 Rockwell International Science Center  
 Thousand Oaks, CA 91360

ABSTRACT

The background and present plans for the ceramics project are reviewed. This provides the framework for the following papers.

Introduction

As was discussed previously, an important element in the development of a quantitative NDE technology is the coupling of nondestructive measurement results, failure modeling, and risk analysis to produce an accept/reject criteria. This basic philosophy was first formulated from first principles in the context of a project to produce a quantitative inspection capability for ceramic materials. In this paper, the history of this project is reviewed and the plans for this year's program, whose results you will hear today, are described

Accept/Reject Criteria

The development of the accept/reject criteria depends on a risk analysis as illustrated in Fig. 1. At the top is an equation for the risk, or cost, associated with the selection of particular accept/reject level. That cost consists of three terms: first term, which is associated with false acceptances, a second term, which is associated with false rejections, and a third, constant term associated with fixed costs. In the equation,  $w_0$  represents the cost of failure (lost in false acceptance),  $w_1$  is the cost of manufacture (lost in false rejection), and  $b$  is the fixed costs. The origin of the probability of false acceptance,  $e_0$ , and the probability of false rejection,  $e_1$ , are illustrated in the graph below. There the probability of a given measurement result,  $y$ , is plotted both for parts which will survive and parts which will fail.

$$R = w_0 e_0 + w_1 e_1 + b$$

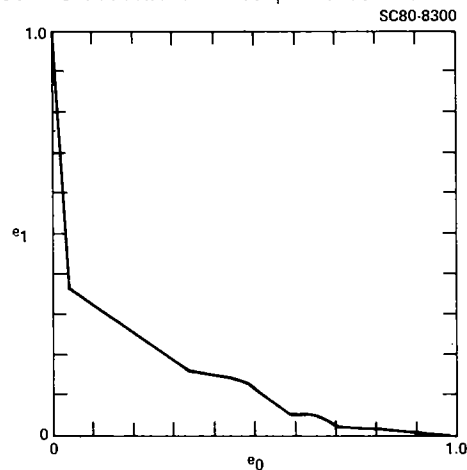
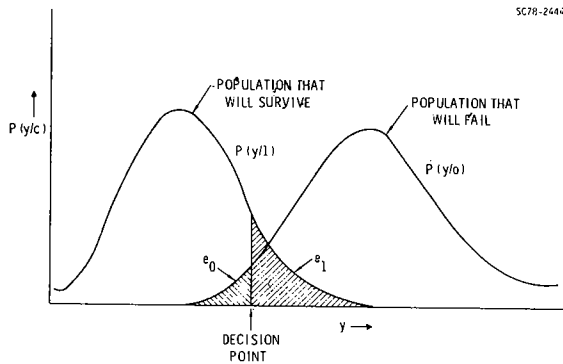


Figure 1. Elements of accept/reject criteria selection (see text for detailed description of figure).

The curve labeled  $P(y/l)$  describes the probability that a given measurement result will be obtained on those parts which will survive. Many of these parts will have a very low NDE indication, or even zero indication, as is illustrated by the fact that the curve extends to low values of  $y$ . A few, however, may produce a fairly large measurement indication. If this exceeds the decision threshold, false rejections of those parts will occur. The probability of false rejection,  $e_1$ , is the cross hatched area under the  $P(y/l)$  curve to the right of the decision point.

Similarly, for that population of parts that will fail, there will be a distribution of measurement results,  $P(y/o)$ . Some of those parts will have measurement results that are lower than the threshold or decision value. Hence, they will be falsely accepted. And, the probability of this is also indicated by a cross hatched area and is equal to  $e_0$ .

As indicated in the upper equation, the risk associated with that particular decision point is equal to the sum of the products of the costs of the false acceptances times the probability of the false acceptances plus the cost of the false rejections times that probability plus the constant term. The optimum decision point is then determined by minimizing the total cost. This amounts to a trade-off between the  $e_0$  and  $e_1$ , the false accept and false reject probabilities. The relative values of those probabilities vary as one changes the decision point. The next graph is an example worked out for one particular case. One can see that either a very high false accept probability accompanied by a low false reject probability, a very high false reject probability accompanied by a low

false accept probability, or some immediate value can be achieved. The particular point on this curve, and thus the decision threshold, is determined by the condition of minimum cost.

#### Available Measurement Techniques

In order to minimize the total cost, the false accept versus false reject curve should lie as close to the axes of the last graph in Fig. 1 as possible. Over the past few years, several techniques have been developed with this objective. Limited evaluations have been performed on a set of disk-shaped  $\text{Si}_3\text{N}_4$  samples containing seeded impurities. This section describes these techniques.

Figure 2 shows a flaw image produced by a scanning laser acoustic microscope (SLAM).<sup>2</sup> From such an image produced in real time, one can make an estimate of the size of the inclusion. This can then be coupled with failure models to produce an estimate of the strength of the part.



Figure 2. SLAM images of Si inclusion in  $\text{Si}_3\text{N}_4$ .

Figure 3 presents results obtained using a high frequency ultrasonic backscattering technique.<sup>3</sup> By analyzing the ultrasonic backscattering in the time domain, one can identify signals corresponding to various ray paths within an inclusion. From these signals, their relative magnitudes and their detailed character in the

time domain, one can make estimates of both the size and material of the inclusion. And, as has been shown in failure modeling,<sup>4</sup> a knowledge of the material as well as the size of the flaw is extremely important in determining whether it will or will not lead to failure.

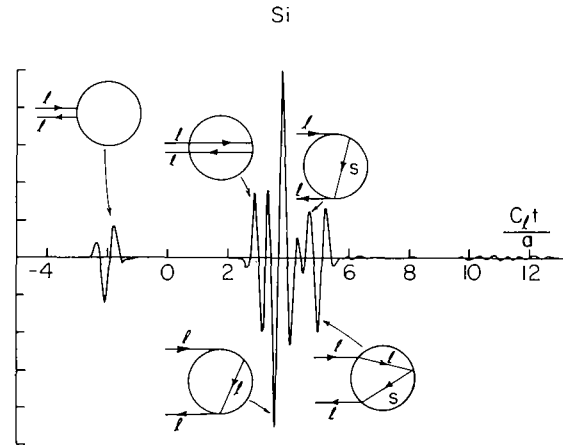


Figure 3. Relative scattering cross-section from Si inclusion in  $\text{Si}_3\text{N}_4$  as a function of time.

A third specimen is illustrated in Fig. 4. Here, statistical estimation theory approach has been used for sizing flaws.<sup>5</sup> This "unified inversion algorithm" makes use of two particular ultrasonic inputs. One input is associated with very low frequency scattering (long wavelength scattering in the Rayleigh regime), and the other is related to the distance from the flaw center to its front surface. From values of these parameters, estimates of flaw size and material are outlined.

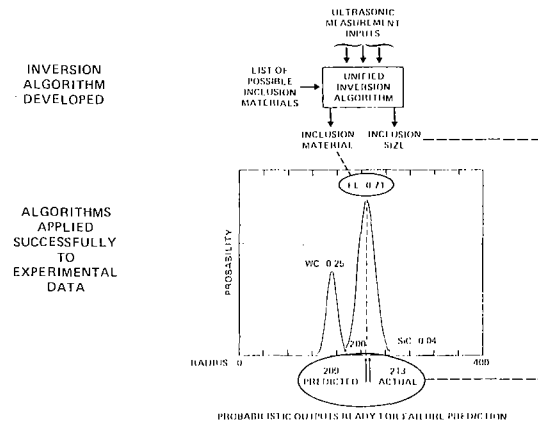


Figure 4. Results of unified inversion algorithm when applied to 200  $\mu\text{m}$  radius Fe inclusion in  $\text{Si}_3\text{N}_4$ .

An important aspect of this approach is that, since it is intrinsically statistical in nature, the output is in the form of a probability distribution. It not only predicts the flaw size and material, but also assigns probabilities and errors to these predictions. In the case shown, there was 71% probability of the detected inclusion being iron, a 25% probability of its being tungsten carbide, and a 4% probability of its being silicon carbide. In fact, it was iron, as was predicted with the highest probability.

Similarly, as shown in the figure, the size predictions are quite accurate. The probabilistic character of the predictions are quite important since, both in the ceramics and metals areas, probabilistic fracture mechanics and life prediction are gaining widespread acceptance. It is going to be very important that NDE techniques also make quantitative probabilistic predictions that can be combined with the probabilistic failure models.

Present Program

The plan for this year, which involves the extension of these ideas to predict strengths of components with naturally occurring flaws, is illustrated in Fig. 5. Starting with the samples, to be discussed below, measurements are being made using the three techniques just discussed. The scanning laser acoustic microscope, high-frequency ultrasonic scattering, and low-frequency ultrasonic scattering. A more generalized inversion algorithm is being developed that will combine all of these inputs to make the best possible estimates of flaw properties. The algorithm will also incorporate inputs from fracture mechanics to make strength prediction. Finally, destructive tests will be made and the predicted strength and the actual or measured strength will be compared.

**PROPOSED WORK FLOW DIAGRAM**

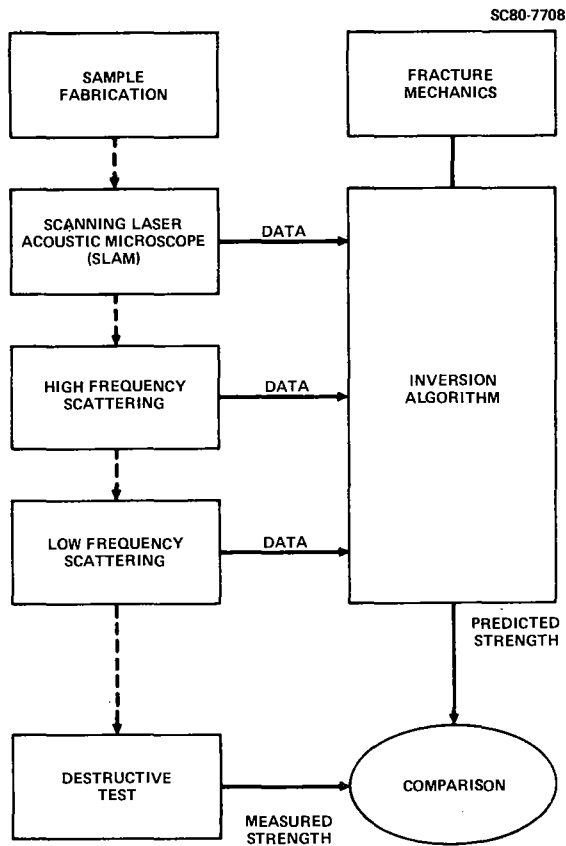
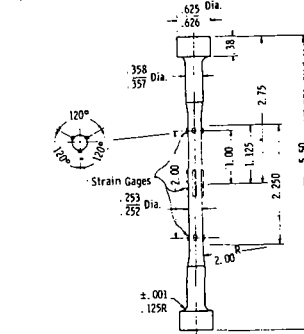


Figure 5. Work flow diagram for ceramics project.

The specimen geometry which has been selected is illustrated in Fig. 6. This is the "button head" specimen which is made from hot pressed silicon nitride. The geometry is particularly suited to destructive tests in a tensile machine.

**"BUTTON HEAD" SILICON NITRIDE**



Strain Gages at Ends of  
Gage Length: .062 in  
Grid Width: .062 in  
Strain Gages at Center of  
Specimens: Gage Length: .50 in  
Grid Width: .060 in

Test specimen dimensions and strain gage locations (1 in. = 25.4 mm; 1 deg = 0.17 rad).

Figure 6. Geometry of "button head" specimen.

The schedule of this effort is illustrated in Fig. 7. Unfortunately, a problem has developed as will be observed by comparing the plan and the actual schedule. Samples were ordered in November and rough billets were received in mid-January, both on schedule. The particular vendor who was doing the final preparation of the button head specimens promised them at the end of April. It was planned that the three different measurement investigators would be able to rotate those samples and complete their data collection by the end of September.

**PROGRAM SCHEDULE**

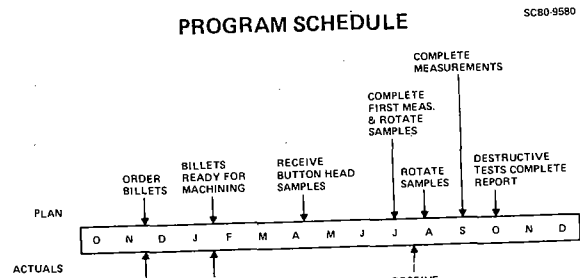


Figure 7. Program schedule.

Unfortunately, the vendor has not yet been able to give us the specimens, and so some of the papers will be less complete than would be desired.

Nevertheless, all the investigators have been developing and refining their techniques. The interim results which are presented give a good indication of what is to come. The results of the final comparison of the destructive tests and the NDE predictions will not be available for a few months.

#### Questions

Unidentified speaker: What materials are you continuing your work with?

Dr. Thompson: Hot-pressed silicon nitride.

Unidentified speaker: Who is the manufacturer of the ceramics?

Dr. Thompson: The ceramic material came from Norton; however, Norton is not doing the machining.

#### References

1. R. Bruce Thompson, "Introductory comments", this proceedings.
2. D. E. Yuhas, T. E. McGraw, and L. W. Kessler, "Scanning laser acoustic microscope visualization of solid inclusions in silicon nitride", Proceedings of the DARPA/AFML Review of Progress in Quantitative NDE, AFWAL-TR-80-4078 (Air Force Wright Aeronautical Laboratories, Dayton, Ohio, 1980), p. 683.
3. C. H. Chou, B. T. Khuri-Yakub, K. Liang, and G. S. Kino, "High-frequency bulk wave measurements of structural ceramics", *ibid*, p. 663.
4. A. G. Evans, M. E. Meyer, K. W. Fertig, B. I. Davis, and H. R. Baumgartner, "Probabilistic models for defect initiated fracture in ceramics", *ibid*, p. 636.
5. L. A. Ahlberg, R. K. Elsley, L. J. Graham, and J. M. Richardson, "Long wavelength ultrasonic characterization of inclusions in silicon nitride", *ibid*, p. 656.

SUMMARY DISCUSSION

Bruce Thompson (Rockwell Science Center [now Ames Laboratory]): So, with that, I think if there are any questions, I would be happy to entertain them; otherwise, we'll go directly into the formal papers.

Unidentified Speaker: What materials are you continuing your work with?

Bruce Thompson: This is a hot-pressed silicon nitride.

Unidentified Speaker: Who is the vendor?

Bruce Thompson: I have debated extensively whether to announce that in public. It was not Norton, from whom we got the billets. We got the billets from Norton, but I suppose I really don't want to pan the vendor in public.

Unidentified Speaker: I was referring to the manufacturer of the ceramics.

Bruce Thompson: The ceramic material came from Norton; however, Norton is not doing the machining on it.

Tony Evans, Chairman (University of California Berkeley): We would like to now start the formal series of papers in this morning's session.